Journal of Geoscience and Environment Protection, 2026, 14(8), 43-62
https://www.scirp.org/journal/gep
ISSN Online: 2327-4344
ISSN Print: 2327-4336

Rock Mass Rating (RMR)-Based Slope Stability Assessment and Geological Hazard Characterization at Kaseve Quarry, Machakos County, Kenya (2015-2024)

Charles Ngala Kithome[1*], Julian A. Ogondo[2], Mary Mwangi[1]

[1]Department of Geology and Meteorology, School of Agriculture, Environment, Water and Natural Resources, South Eastern Kenya University (SEKU), Kitui, Kenya
[2]Department of Geography and Natural Resource Management, School of Arts and Social Sciences, Maseno University, Kisumu, Kenya
Email: *charliekithome@gmail.com

How to cite this paper: Kithome, C. N., Ogondo, J. A., & Mwangi, M. (2026). Rock Mass Rating (RMR)-Based Slope Stability Assessment and Geological Hazard Characterization at Kaseve Quarry, Machakos County, Kenya (2015-2024). *Journal of Geoscience and Environment Protection, 14,* 43-62.
https://doi.org/10.4236/gep.2026.148003

Received: July 7, 2026
Accepted: August 11, 2026
Published: August 14, 2026

Abstract

Quarrying in structurally complex crystalline rocks can create significant instability hazards where steep excavation faces intersect persistent discontinuities and seasonal groundwater. This study assessed five representative wall sections at Kaseve Quarry, Machakos County, Kenya, using the Bieniawski Rock Mass Rating (RMR89) system, field structural observations, laboratory-derived strength parameters, historical incident records and SLOPE/W-derived dry- and wet-condition factors of safety (FS). Historical management records for 2015-2021 were used to reconstruct rockfall and blasting histories, while field, laboratory and groundwater investigations were undertaken from January 2022 to March 2024. After analyzed of the discrete RMR89 ratings, wall-scale RMR values ranged from 28 at the Back Wall to 49 at the East Wall, classifying the investigated rock masses as Poor to Fair. Reported dry-condition FS values ranged from 1.08 to 1.68, while wet-condition values ranged from 0.82 to 1.35. The Back and South walls recorded wet-condition FS values below 1.0 and also exhibited the most pronounced cracking, seepage and historical rockfall evidence. Using the corrected RMR values and the SLOPE/W-derived dry FS dataset, exploratory ordinary least-squares regression gave FS = 0.0254RMR + 0.399 (R2 = 0.938; r = 0.968; p = 0.0067; n = 5). Because FS is a calculated response and the sample contains only five wall-scale units, this relationship is interpreted as site-specific rather than predictive. The integrated evidence identifies the Back and South walls as the highest-priority areas for drainage improvement, re-benching, controlled blasting and systematic displacement and groundwater monitoring.

Keywords

Rock Mass Rating (RMR), Slope Stability, Limit-Equilibrium Analysis, Geological Hazards, Quarry Engineering

1. Introduction

Quarrying operations are indispensable to infrastructure development globally, supplying raw construction materials critical to urbanization. However, the mechanical disturbance of rock masses through excavation and blasting generates significant geotechnical hazards, most notably slope instability that poses life-threatening risks to workers and surrounding communities (Bieniawski, 1989). In Sub-Saharan Africa, the rapid expansion of small- to medium-scale quarrying operations has outpaced the implementation of geotechnical regulation, creating a critical gap between industrial practice and slope safety management.

Rock Mass Rating (RMR), developed by Bieniawski (1989), remains the most widely adopted empirical geotechnical classification system globally, offering a structured quantification of rock mass quality through six weighted parameters: uniaxial compressive strength (UCS), rock quality designation (RQD), discontinuity spacing, discontinuity condition, groundwater state, and discontinuity orientation adjustment (Fredrick et al., 2023). When integrated with the Factor of Safety (FS) framework using the Mohr-Coulomb failure criterion, RMR-based analysis enables rigorous quantitative slope stability assessment applicable to diverse geological settings (Fritz et al., 2013).

Kaseve Quarry, located in Machakos County, Kenya, operates within the Precambrian crystalline basement of the Mozambique Belt, a geologically complex terrane characterized by polyphase deformation, pervasive foliation, and intense jointing (Indiatsy, 2018). Despite over two decades of continuous quarrying activity and documented slope failures between 2015 and 2024, no systematic geotechnical characterization has been conducted. This absence represents both a scientific gap and a regulatory failure, as quarry operators lack evidence-based parameters for slope design or hazard mitigation.

This study addresses Objective 2 of a broader geohazard assessment programme at Kaseve Quarry by evaluating slope stability using the Rock Mass Rating (RMR) system and characterizing geological hazards over the period 2015-2024. The investigation integrates two complementary sources of evidence. Historical quarry management records (2015-2021) were used to reconstruct the chronology of rockfalls, blasting activities, and reported slope instability events, whereas geotechnical field investigations undertaken between 2022 and 2024 provided the primary data for RMR classification, slope geometry, laboratory-derived rock strength parameters, groundwater observations, and Factor of Safety (FS) analyses. Specifically, the study aimed to: 1) classify the rock mass quality of the five active quarry wall sections; 2) evaluate slope stability under dry and rainfall-induced saturated conditions using FS analysis; 3) examine the site-specific relationships between RMR, slope angle, and FS; and 4) integrate analytical results with historical records and field observations to identify and prioritize areas requiring geotechnical intervention. Owing to the limited number of independent quarry wall sections, comparisons between failure-prone and relatively stable walls are presented descriptively to support engineering interpretation.

2. Study Area

2.1. Location and Physical Setting

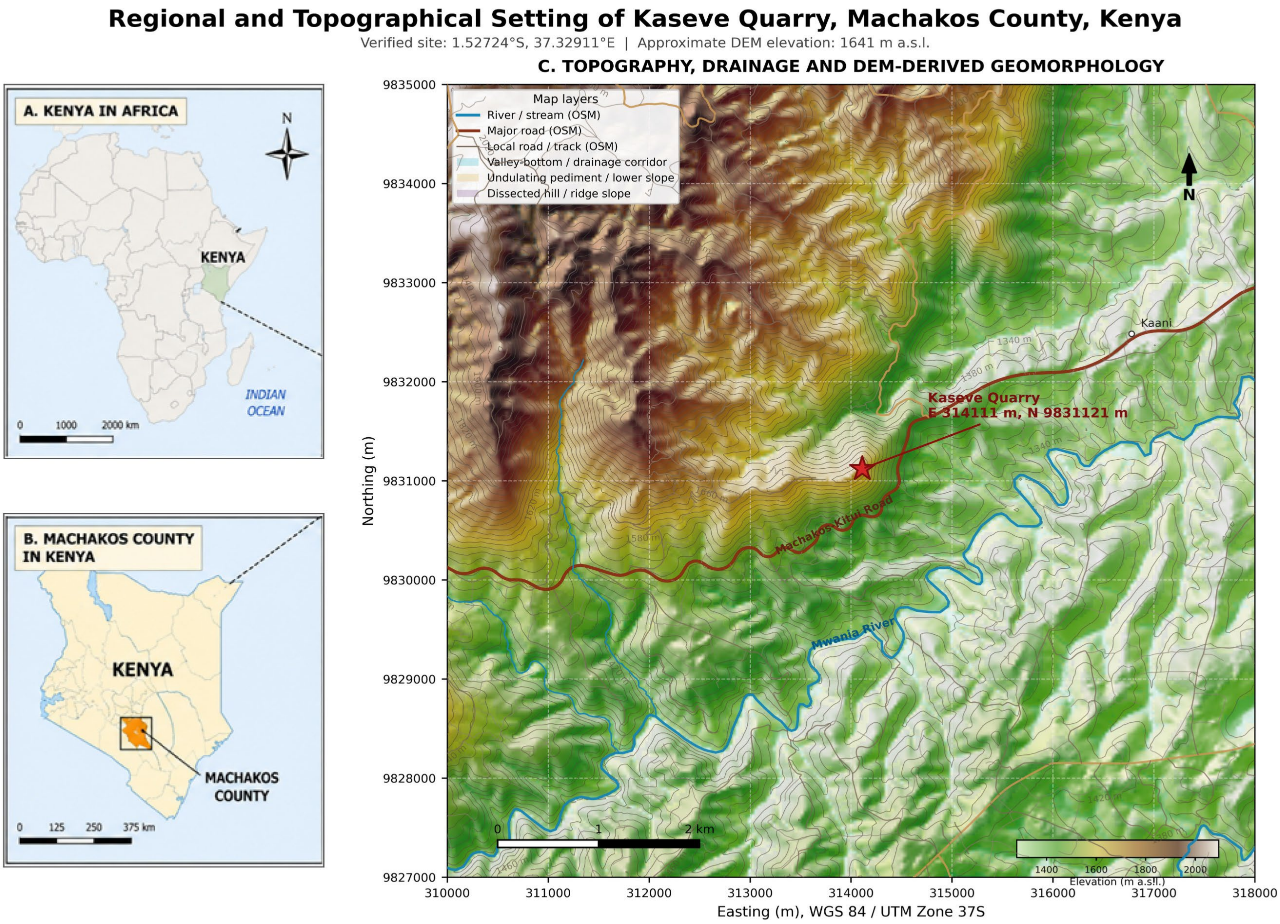

Figure 1. Regional and topographical setting of Kaseve Quarry, Machakos County, Kenya. Panels A-B show the continental and county settings; Panel C overlays Copernicus DEM GLO-30 hillshade and 20 m contours with OpenStreetMap drainage, roads and settlements. The geomorphological units are DEM-derived morphometric classes based on slope and topographic position and require field verification.

Kaseve Quarry is situated approximately 7 km east of central Machakos Town in Machakos County, Kenya, at the verified WGS 84/UTM Zone 37S control point E 314111 m, N 9831121 m (1.52724˚S, 37.32911˚E). Copernicus GLO-30 indicates an elevation of approximately 1641 m a.s.l. at the control point (**Figure 1**). The surrounding terrain is a dissected basement-rock highland comprising ridges, undulating lower slopes and incised drainage corridors rather than a uniform plain. The quarry occupies approximately 3.2 hectares in a semi-arid landscape where seasonal rainfall can elevate pore-water pressure within persistent discontinuities.

Kaseve Quarry has been in active operation since approximately 2001, primarily extracting crushed stone aggregates for road construction and building materials supply to Nairobi and Machakos urban centres. By 2024, the quarry had excavated to an average depth of 22 m, with the deepest section (Back Wall) reaching 28 m. Five distinct wall sections—North, South, East, West, and Back—represent the primary geotechnical investigation units of this study, each presenting unique combinations of slope angle, height, rock mass quality, and failure mode.

Coordinate Reference and Map Control

The quarry control point is E 314111 m, N 9831121 m in WGS 84/UTM Zone 37S, equivalent to 1.52724˚S, 37.32911˚E. Figure 1 applies this control to a terrain-based map integrating DEM hillshade, 20 m elevation contours, drainage, roads, settlements and DEM-derived geomorphological units. Figure 2 provides the detailed geological and structural map of the quarry.

2.2. Geological Setting

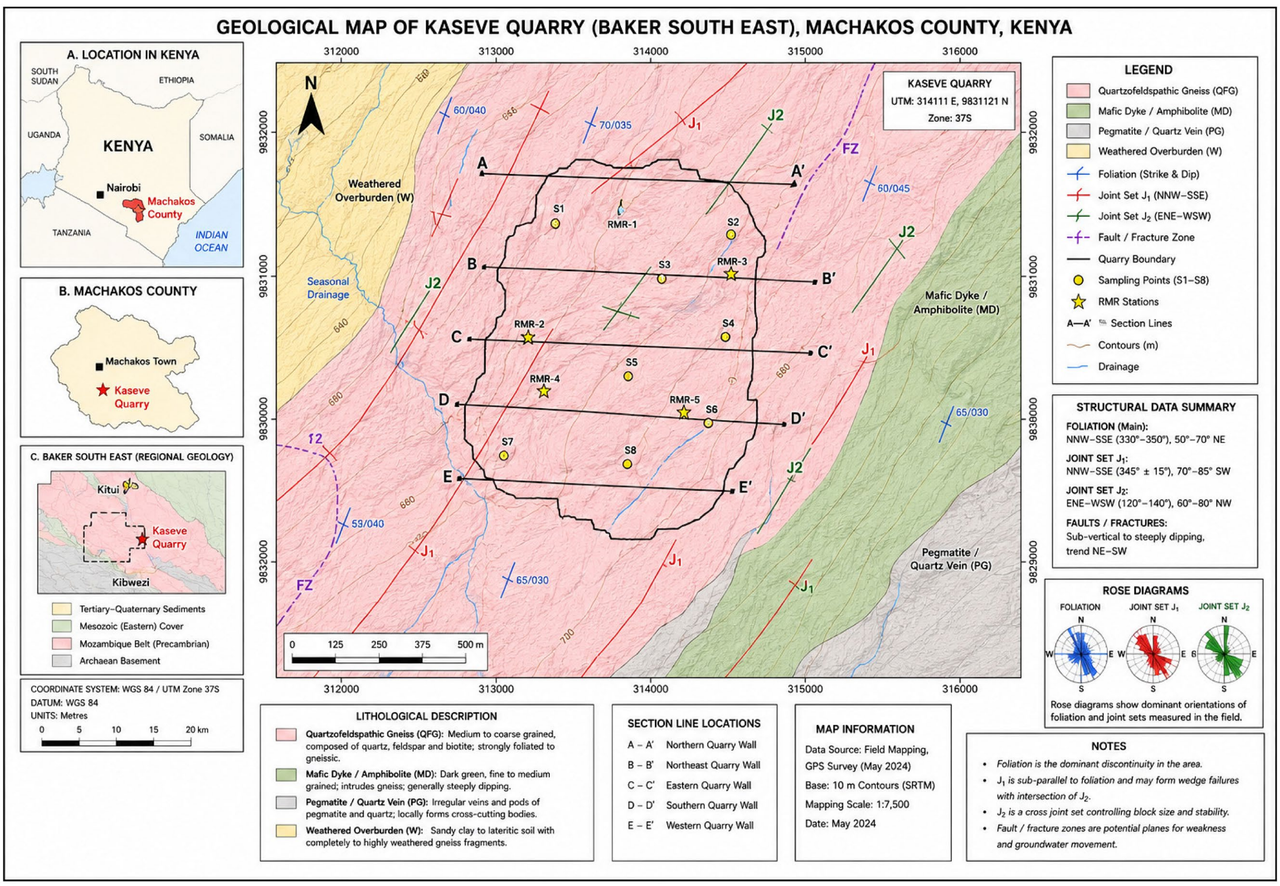

Figure 2. Geological and structural map of Kaseve Quarry showing the principal lithological units, quarry boundary, sampling stations, mapped discontinuities and section traces A-A' to E-E'. Insets show the national, county and regional geological settings.

Kaseve Quarry is underlain by Precambrian crystalline basement rocks of the Mozambique Belt, a major Pan-African orogenic suture zone extending from Ethiopia through Kenya to Mozambique (Mathu, 1992) as shown in **Figure 2**. The Machakos segment of the belt records multiple phases of Neoproterozoic deformation (900 - 540 Ma), resulting in folding, tilting, and subsequent metamorphism into crystalline schists, gneisses, and granulites (Mathu, 1992). The predominant rock type exposed at Kaseve Quarry is biotite gneiss characterized by well-developed foliation (strike N10˚ - 30˚E; dip 45˚ - 65˚NW), closely spaced joints, and progressive near-surface weathering (Indiatsy, 2018).

Three primary joint sets have been mapped: Set J1 (strike N10˚E, dip 62˚NW, spacing 12 - 30 cm), Set J2 (strike N85˚E, dip 45˚SE, spacing 20 - 45 cm), and Set J3 (sub-horizontal, dip 5˚ - 12˚NW, spacing 40 - 80 cm). The intersection of J1 and J2 creates wedge-failure potential at the East and West Walls, while the sub-horizontal J3 set, combined with steeply dipping foliation, creates planar-failure conditions at the Back Wall. Three major fault structures transect the quarry: the Kaseve Normal Fault (N20˚E, dip 70˚NW), the Cross Fault (N80˚E, dip 55˚SE), and a secondary synthetic splay of the Mutito Fault System (Nyamai et al., 2004).

3. Methodology

Systematic geotechnical field surveys were conducted across five quarry wall sections between January 2022 and March 2024. Rock strength was determined in situ using an N-type Schmidt rebound hammer (minimum 20 readings per site, with Deere and Miller (1966) correlation applied to derive UCS). Rock quality designation (RQD) was estimated from borehole cores (three BQ-size vertical boreholes, 15 - 20 m depth each) and supplemented by the Palmström (1982) volumetric joint count method from scanline surveys. Discontinuity spacing, condition (roughness, aperture, infilling, and weathering), and groundwater state were recorded following the ISRM Suggested Methods compiled by Ulusay and Hudson (2007). Structural measurements were obtained using a Clar-type Brunton compass with a minimum of 30 readings per wall section.

Slope geometry parameters (angle, height, bench configuration) were measured using a total station survey (Leica TS06 Plus) with 5 cm accuracy, supplemented by drone photogrammetry (DJI Phantom 4 Pro) processed with Agisoft Metashape to produce 3D point clouds. Laboratory testing on representative core samples determined bulk density, effective cohesion (c'), and internal friction angle (φ') using direct shear and triaxial compression tests. Pore water pressure measurements during the short rain season (October-December 2023) were obtained using standpipe piezometers installed at three monitoring locations.

3.1. Construction of the 2015-2024 Dataset

The ten-year study period was not treated as a continuous instrumental monitoring record. It was constructed by combining (a) historical quarry-management incident and blasting logs for 2015-2021 and (b) direct field, laboratory, and groundwater measurements collected from January 2022 to March 2024. Historical records were used only for the chronology and frequency of rockfalls, blasting, and reported slope distress. They were not used to generate RMR ratings, laboratory shear-strength parameters, slope geometry, piezometric pressure, or FS. Crack apertures and widening rates reported for 2022-2024 were derived from field markers and repeat measurements.

3.2. Field Sampling and Wall-Scale Aggregation

Each wall was investigated using two scanlines positioned to capture the dominant exposed structural domains, giving 10 scanlines. Twenty valid N-type Schmidt rebound readings were retained per wall after removal of obvious outliers and correction for hammer orientation, giving 100 readings as shown in **Table 1**. Structural mapping comprised 30 discontinuity measurements per wall (150 measurements), including dip, dip direction, spacing, persistence, aperture, roughness, infilling, and weathering. Three BQ-size boreholes, 15 - 20 m deep, were positioned adjacent to the South, East and Back walls. Six logged core intervals from each borehole were used, giving 18 intervals. The North and West walls had no directly adjacent core; their RQD values were estimated from scanline-based volumetric joint counts using the Palmström relationship, while nearby core provided only a lithological consistency check.

Slope angle, height, and bench geometry were measured by total station and checked using drone photogrammetry. Laboratory tests on representative core specimens determined bulk unit weight, effective cohesion, and effective friction angle. For each wall, rebound-derived UCS values were represented by the median; discontinuity observations were summarized by the modal RMR category, adopting the more conservative category where adjacent classes were equally represented. For cored walls, core and scanline RQD were reconciled and the lower representative rating was selected where the two differed materially. The six RMR components were summed once to produce one wall-scale score.

Table 1. Wall-specific sampling effort and data sources used in the 2022-2024 geotechnical assessment.

Wall	Scanlines	Valid rebound readings	Structural measurements	Core intervals	RQD basis
North	2	20	30	0	Palmström scanline estimate||
South	2	20	30	6	BQ core + scanline reconciliation
East	2	20	30	6	BQ core + scanline reconciliation
West	2	20	30	0	Palmström scanline estimate
Back	2	20	30	6	BQ core + scanline reconciliation
Total	10	100	150	18	-

3.3. Rock Mass Rating Classification

RMR was computed following Bieniawski (1989) through summation of six weighted ratings:

$$\text{RMR} = \text{R}_1 + \text{R}_2 + \text{R}_3 + \text{R}_4 + \text{R}_5 + \text{R}_6 \quad (1)$$

where R_1 = UCS rating (0 - 15); R_2 = RQD rating (3 - 20); R_3 = discontinuity spacing rating (5 - 20); R_4 = discontinuity condition rating (0 - 30); R_5 = groundwater rating (0 - 15); R_6 = orientation adjustment (−60 to 0). Total RMR scores classify rock mass quality: RMR < 40 = Poor (Class IV); 40 - 60 = Fair (Class III); 61 - 80 = Good (Class II); 81 - 100 = Very Good (Class I). Arithmetic totals were verified against the individual component ratings before statistical analysis.

3.4. Factor of Safety Analysis Using SLOPE/W

3.4.1. Model Definition and Input Parameters

Factor-of-safety analyses were performed in GeoStudio SLOPE/W using two-dimensional limit-equilibrium models of representative cross-sections through the five quarry walls. Measured wall height and face angle defined the external geometry. Each wall was represented as an equivalent Mohr-Coulomb material using the effective cohesion (c'), effective friction angle (φ') and bulk unit weight (γ).

The critical Factor of Safety was evaluated using the Morgenstern-Price formulation with an automated search for the minimum admissible slip surface. SLOPE/W expresses FS as the ratio of available shear resistance to the mobilized shear force required for limiting equilibrium:

$$\text{FS} = \frac{\Sigma\left[c'\Delta l + N'\tan\left(\varphi'\right)\right]}{\Sigma T} \quad (2)$$

where Δl is the base length of a slice, N' is the effective normal force and T is the mobilized shear force. The calculation integrates the complete trial surface and slice-force equilibrium; it is therefore not equivalent to a single-plane screening equation.

3.4.2. Hydraulic Scenarios, Search Geometry and Interpretation

Two hydraulic scenarios were analysed. Dry-condition models assigned zero pore-water pressure. Wet-condition models incorporated the peak seasonal pore-pressure values through the corresponding piezometric surface or equivalent pore-pressure distribution. All other material and geometric inputs were held constant between scenarios.

The search geometry was conditioned by the mapped failure mechanism. Planar and non-circular trial surfaces were examined where persistent foliation or discontinuities daylighted in the wall; circular and composite surfaces were examined at the deeply weathered Back Wall. Wedge and toppling potential was identified separately from structural measurements and field evidence. The reported SLOPE/W values are consequently two-dimensional wall-scale screening values rather than three-dimensional wedge or toppling solutions.

The calculations assumed unit out-of-plane thickness, representative homogeneous strength within each modelled wall section, no seismic loading and no stabilizing support. FS ≥ 1.5 was treated as meeting the adopted dry-condition target margin; 1.0 ≤ FS < 1.5 as marginal; and FS < 1.0 as calculated instability under the analysed scenario. These are study screening criteria, not RMR class boundaries.

3.5. Pore-Pressure Derivation from Piezometric Readings

Standpipe piezometers at the North, South, and East monitoring locations recorded groundwater depths of 2.1 m, 4.2 m, and 0.7 m below the wall crest, respectively, during the October-December 2023 monitoring period. Pore-water pressures (u, kPa) were calculated as

$$u = \gamma_w h_w \tag{3}$$

where γ_w = 9.81 kN/m^3 and h_w is the height of the groundwater column above the representative failure plane. Measured pore-water pressures were 42 kPa (North Wall), 58 kPa (South Wall), and 31 kPa (East Wall). For the West and Back Walls, where piezometers were not installed, pore-water pressures of 44 kPa and 72 kPa, respectively, were estimated using inverse-distance interpolation constrained by relative elevation, observed seepage conditions, topographic position, and groundwater continuity inferred from the geological structure. These values represent peak wet-season conditions and were adopted for the saturated stability analyses rather than long-term average groundwater conditions.

3.6. Statistical Analysis

Each quarry wall was treated as one independent engineering unit, yielding five wall-scale observations. Descriptive statistics summarized corrected RMR89, SLOPE/W-derived Factor of Safety, wall geometry and mapped geological hazards. Inferential calculations were performed using two-sided tests with $\alpha = 0.05$.

3.6.1. Ordinary Least-Squares Linear Regression

Ordinary least-squares (OLS) regression evaluated the site-specific linear association between corrected RMR89 (predictor, x) and dry-condition SLOPE/W-derived Factor of Safety (response, y). Each quarry wall contributed one paired observation. The fitted model followed:

$$\text{FS}_i = \beta_0 + \beta_1 \text{RMR}_i + \varepsilon_i \tag{4}$$

where FS_i and RMR_i are the paired values for wall i, β_0 is the intercept, β_1 is the regression slope and ε_i is the residual. Reporting included β_0, β_1, the slope standard error and 95% confidence interval, the coefficient of determination (R^2), residual standard error and sample size.

3.6.2. Pearson Product-Moment Correlation

Pearson's product-moment correlation coefficient quantified the direction and strength of the linear association between corrected RMR89 and dry-condition FS using the same five paired wall observations:

$$r = \frac{\Sigma\left[\left(x_i - \bar{x}\right)\left(y_i - \bar{y}\right)\right]}{\sqrt{\left[\Sigma\left(x_i - \bar{x}\right)^2 \Sigma\left(y_i - \bar{y}\right)^2\right]}} \tag{5}$$

where x denotes corrected RMR89, y denotes dry-condition FS, and the overbars denote sample means. A two-sided test of H_0: $\rho = 0$ used $t = r\sqrt{\left[\left(n-2\right)/\left(1-r^2\right)\right]}$ with $n-2$ degrees of freedom. An approximate 95% confidence interval for r was obtained using the Fisher z transformation.

3.6.3. Statistical Scope and Limitations

The regression and correlation are exploratory because n = 5 and all observations originate from one quarry. Normality tests and formal outlier rejection were not applied because five observations cannot support meaningful distributional diagnostics. RMR-related strength and rock-mass characteristics also contribute to the SLOPE/W model inputs, so the association is partly model-structured and does not constitute independent predictive validation. No training-validation split, external calibration or causal interpretation was attempted.

3.7. Qualitative Hazard-Prioritization Matrix

Likelihood ranks from 1 (very low) to 5 (very high) were assigned using corrected RMR, wet-condition FS, mapped cracking and deformation, groundwater response and rockfall history. Consequence ranks from 1 (insignificant) to 5 (catastrophic) considered wall height and geometry, potential failure volume, runout and exposure of personnel, equipment and quarry operations. The matrix is an ordinal site-screening tool; the ranks are engineering judgements rather than failure probabilities.

4. Results

4.1. Geotechnical Characterization and RMR Assessment

Corrected Rock Mass Rating (RMR89) values for the five quarry wall sections ranged from 28 at the Back Wall to 49 at the East Wall (**Tables 2-4**; **Figure 3**). The Back (RMR = 28), South (RMR = 30) and North (RMR = 39) walls are Class IV (Poor rock), whereas the West (RMR = 42) and East (RMR = 49) walls are Class III (Fair rock). The lower ratings at the Back and South walls reflect the combined effects of lower intact-rock strength, closer discontinuity spacing, poorer discontinuity condition and groundwater. These corrected classifications are used throughout the stability and hazard assessment.

Table 2. Corrected RMR89 component ratings and rock-mass classes for the five quarry walls.

RMR Parameter	North Wall	South Wall	East Wall	West Wall	Back Wall
R1: UCS (MPa)	45 MPa → 4	38 MPa → 4	62 MPa → 7	55 MPa → 7	32 MPa → 4
R2: RQD (%)	55% → 13	48% → 8	72% → 13	65% → 13	38% → 8
R3: Disc. spacing	15 cm → 8	10 cm → 8	22 cm → 10	18 cm → 8	8 cm → 8
R4: Disc. condition	12	10	14	12	8
R5: Groundwater	7	5*	10	7	5*
R6: Orientation adj.	−5*	−5*	−5*	−5*	−5*
Total RMR	39	30	49	42	28
Classification	Poor (Class IV)	Poor (Class IV)	Fair (Class III)	Fair (Class III)	Poor (Class IV)

Source: Field survey data (2022-2024); RMR classification after Bieniawski (1989). *Groundwater and orientation ratings represent the wall-scale values adopted in the final RMR89 assessment. Orientation adjustments should be interpreted together with the mapped discontinuity geometry and wall-specific failure mechanisms presented in the study.

Table 3. Wall geometry, effective-strength parameters, unit weights and adopted wet-season pore pressures used in SLOPE/W.

Wall Section	Slope Angle (˚)	Height (m)	c'(kPa)	φ'(˚)	γ (kN/m³)	u_sat (kPa)
North Wall	65	18	28	34	26.5	42
South Wall	72	20	22	28	25.8	58
East Wall	58	15	35	38	27.2	31
West Wall	68	17	30	35	26.8	44
Back Wall	75	28	18	25	25.5	72

Notes: c'= effective cohesion; φ'= effective friction angle; γ = bulk unit weight; u_sat = saturated pore pressure. Laboratory testing on BQ core samples (2022-2024). Pore pressures (u_sat): North, South, East walls measured via standpipe piezometers (Oct-Dec 2023); West and Back Wall values assigned from relative elevations, proximity, seepage patterns, and groundwater continuity.

Table 4. Corrected RMR89 classification, hazard priority and principal interpreted failure mode.

Wall	RMR	Class	UCS (MPa)	RQD (%)	Spacing (cm)	Priority	Mode
North	39	Poor IV	45	55	15	Moderate	Wedge/toppling
South	30	Poor IV	38	48	10	Very high	Planar/wedge
East	49	Fair III	62	72	22	Low	Wedge
West	42	Fair III	55	65	18	Moderate	Wedge/planar
Back	28	Poor IV	32	38	8	Very high	Planar/circular

Source: Field RMR classification, January 2022-March 2024.

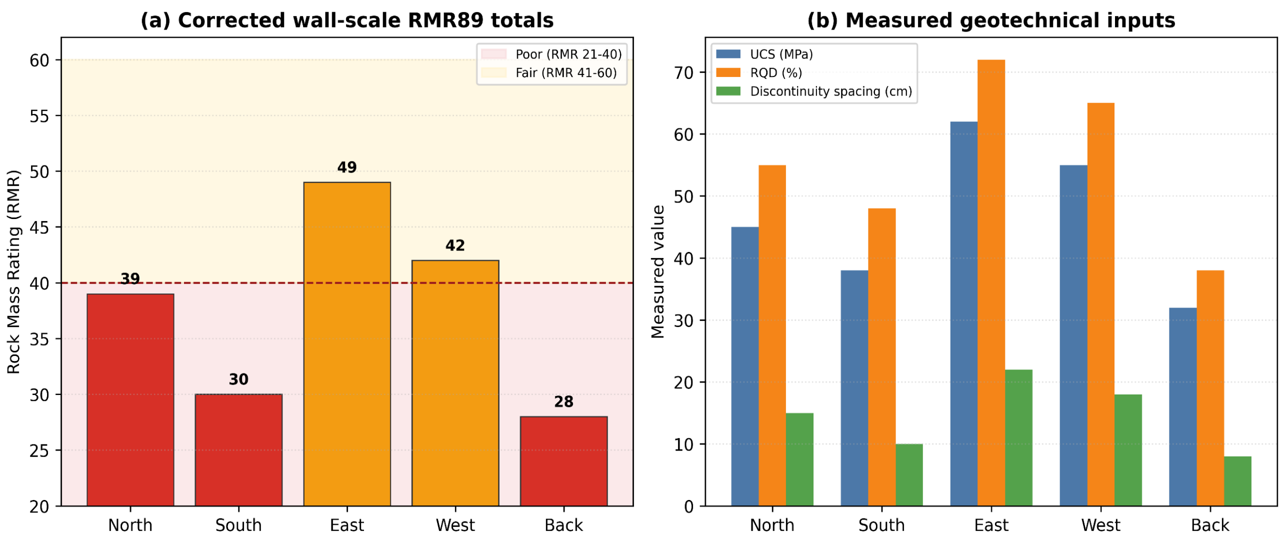

Figure 3. (a) Corrected RMR89 totals for the five quarry walls and (b) measured intact-rock strength, RQD and discontinuity spacing. RMR 21 - 40 is Class IV (Poor) and RMR 41-60 is Class III (Fair); groundwater and orientation components are subject to the Table 2 verification note.

4.2. Factor of Safety under Dry Conditions

Under dry conditions (u = 0), FS values ranged from 1.08 (Back Wall) to 1.68 (East Wall), reflecting the relative influence of slope geometry, cohesion, and friction angle across sections (Table 5). The North Wall (FS = 1.42) and West Wall (FS = 1.38) were classified as marginally stable (1.0 ≤ FS < 1.5), while the South Wall (FS = 1.21) and Back Wall (FS = 1.08) approached critical thresholds. Only the East Wall (FS = 1.68) achieved acceptable stability margins under dry conditions, as illustrated in Figure 4.

Table 5. SLOPE/W-derived dry-condition Factor of Safety and screening interpretation.

Wall Section	RMR	Slope Angle (˚)	Height (m)	c'(kPa)	φ′(˚)	FS (Dry)	Stability Status
East Wall	49	58	15	35	38	1.68	Stable
North Wall	39	65	18	28	34	1.42	Marginally Stable
West Wall	42	68	17	30	35	1.38	Marginally Stable
South Wall	30	72	20	22	28	1.21	Marginally Stable
Back Wall	28	75	28	18	25	1.08	Marginally Stable

Note: Adopted dry-condition screening interpretation: FS < 1.0 = Unstable; 1.0 ≤ FS < 1.5 = Marginal; FS ≥ 1.5 = Stable.

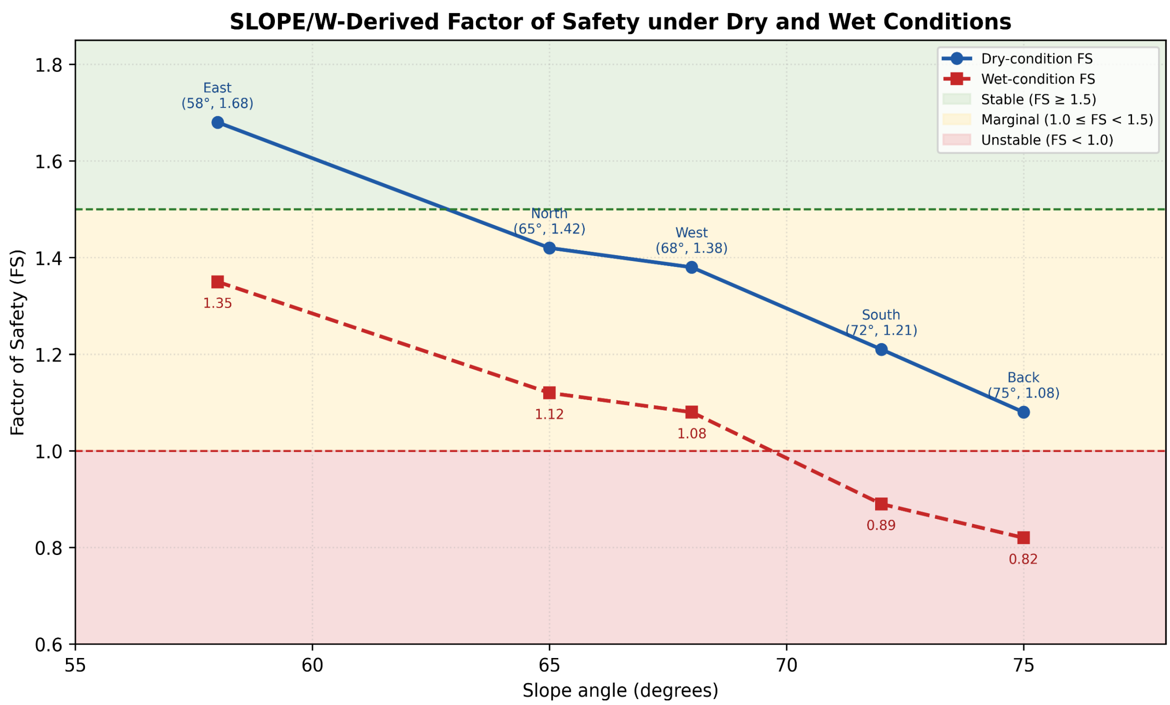

Figure 4. SLOPE/W-derived Factor of Safety versus wall angle under dry and adopted wet conditions. The horizontal reference lines show FS = 1.0 and the adopted target margin FS = 1.5.

4.3. Factor of Safety—Saturated Conditions

Under saturated conditions, all FS values declined substantially relative to dry conditions, with reductions ranging from ΔFS = 0.33 (East Wall) to ΔFS = 0.26 (Back Wall). Critically, both the Back Wall (FS = 0.82) and South Wall (FS = 0.89) fell below the failure threshold of FS = 1.0, indicating calculated instability under the adopted wet-condition scenario during seasonal peak rainfall events as summarized in Table 6 and illustrated in Figure 5. The West Wall (FS = 1.08, wet) also approached critical conditions.

Table 6. SLOPE/W-derived dry- and wet-condition Factors of Safety and wet-condition screening interpretation.

Wall section	Slope angle (˚)	Height (m)	FS (dry)	FS (wet)	Delta FS	Wet-condition interpretation
East Wall	58	15	1.68	1.35	0.33	Marginal
North Wall	65	18	1.42	1.12	0.30	Marginal
West Wall	68	17	1.38	1.08	0.30	Marginal
South Wall	72	20	1.21	0.89	0.32	Unstable
Back Wall	75	28	1.08	0.82	0.26	Unstable

Note: ΔFS is the reduction from dry to wet conditions. Adopted screening interpretation: FS < 1.0 = Unstable; 1.0 ≤ FS < 1.5 = Marginal; FS ≥ 1.5 = Stable.

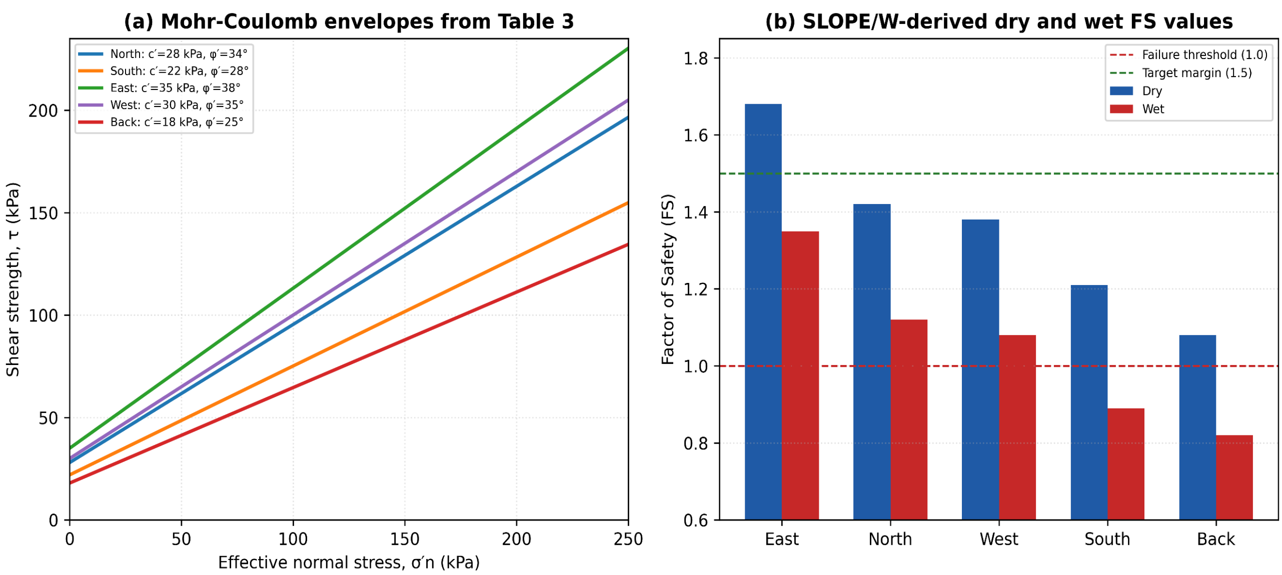

Figure 5. (a) Mohr-Coulomb failure envelopes calculated from the effective cohesion and friction angle in Table 3 and (b) SLOPE/W-derived dry- and wet-condition Factors of Safety for all five walls.

4.4. Geological Hazard Evidence at Kaseve Quarry (2015-2024)

Field investigations documented active geological hazard manifestations consistent with the analytical instability findings. Tension cracks measuring 8 - 12 m behind the Back Wall crest and 5 - 8 m behind the South Wall crest were mapped, with maximum measured apertures of 8.5 cm (Back Wall, 2023 survey) and 5.2 cm (South Wall, 2023). Progressive widening of 1.2 - 2.4 cm/year was measured relative to 2022 reference markers, indicating ongoing slope creep (Table 7). Historical failure records from quarry-management logs document seven rockfall events at the Back Wall between 2015 and 2021. The temporal association of individual events with rainfall was not independently verified in the present analysis.

Table 7. Field geological-hazard evidence and recorded rockfalls for the five quarry walls.

Wall	Crack distance (m)	Max aperture (cm)	Widening (cm/yr)	Recorded rockfalls (2015-2021)	Observed mode
Back	8 - 12	8.5	2.4	7	Planar + toppling
South	5 - 8	5.2	1.8	5	Planar
West	3 - 5	3.8	1.2	3	Wedge
North	2 - 4	2.5	0.8	2	Minor wedge
East	None	N/A	N/A	0	None

Source: Summary of Geological Hazard Evidence (Historical records 2015-2021 and field observations 2022-2024); *Historical failure records (2015-2021) from quarry management logs; primary field and laboratory investigations 2022-2024.

4.5. Interpretive Wall-Scale Kinematic Illustrations

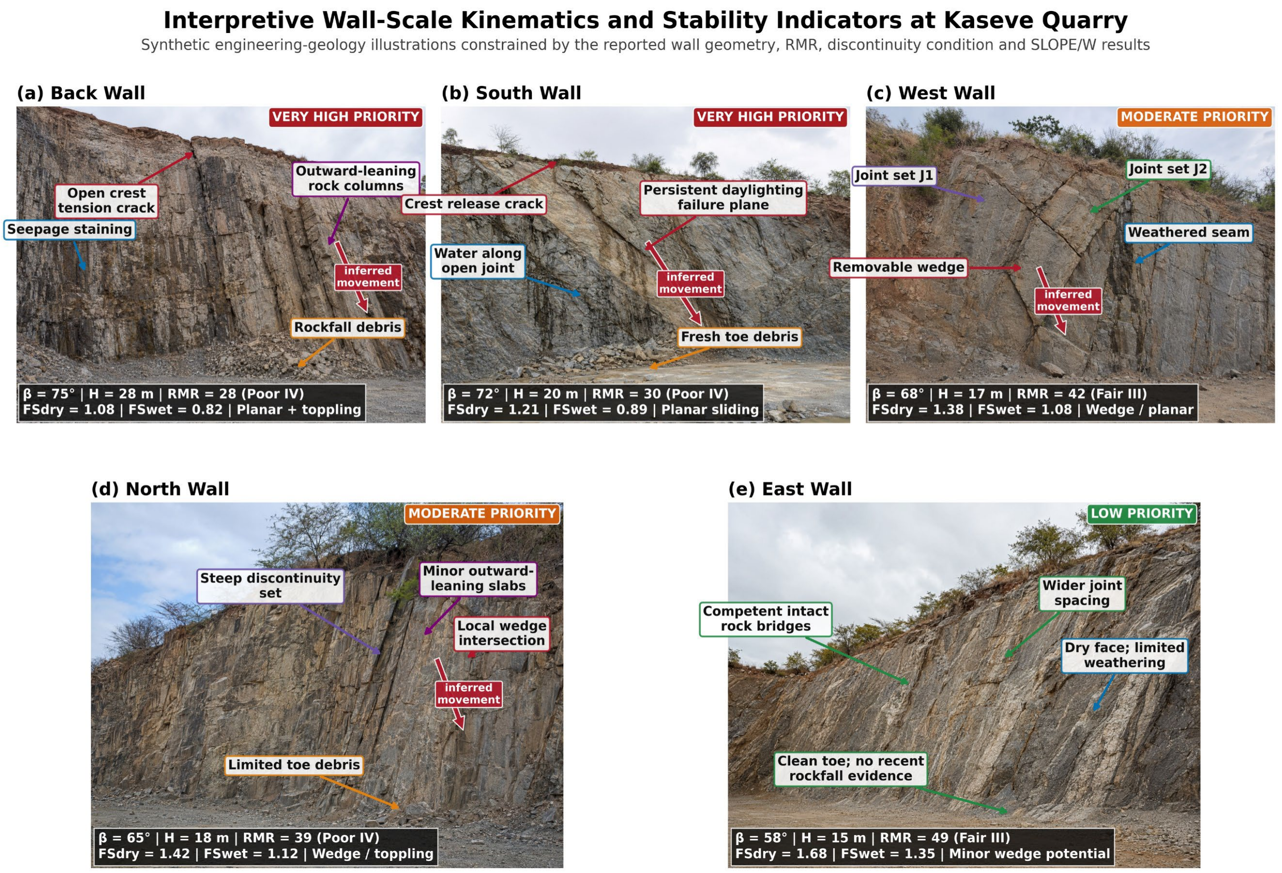

Figure 6. Interpretive engineering-geology illustrations of (a) Back, (b) South, (c) West, (d) North and (e) East walls. Panel annotations demonstrate the inferred critical discontinuities, moisture indicators and likely movement directions using the wall geometry, corrected RMR89 and SLOPE/W-derived FS values reported in Tables 2-7. These panels are conceptual explanatory illustrations, not original site photographs, new field evidence or quantitative photogrammetry.

Because the available field photographs were insufficiently sharp for publication-scale structural demonstration, Figure 6 uses engineering-geology illustrations constrained by the measured wall geometry and the RMR, discontinuity, groundwater and SLOPE/W results from Tables 2-7. The Back Wall panel demonstrates closely spaced discontinuities, a crest release crack, seepage staining and combined planar-toppling potential. The South Wall illustrates a persistent daylighting plane and inferred planar movement. The West Wall demonstrates a removable wedge formed by intersecting joint sets. The North Wall shows local wedge and minor toppling geometries, while the East Wall shows wider joint spacing, competent rock bridges and limited weathering. These panels explain the interpreted mechanisms but do not constitute new field observations, measured photogrammetry or evidence of features not recorded in the dataset.

4.6. RMR-FS Regression and Pearson Correlation Analysis

4.6.1. Ordinary Least-Squares Regression Results

The OLS analysis used five wall-scale pairs of corrected RMR89 and dry-condition FS: East (49, 1.68), North (39, 1.42), West (42, 1.38), South (30, 1.21) and Back (28, 1.08). The fitted site-specific relationship shown in Figure 7 was:

$$FS = 0.0254 \times RMR + 0.399$$

The regression slope was 0.02539 FS units per RMR point (standard error = 0.00378; 95% CI: 0.01336 - 0.03743). The model explained 93.76% of the observed dry-condition FS variation ($R^2 = 0.9376$), with a residual standard error of 0.0656 FS units (n = 5). Within this dataset, a one-point increase in corrected RMR corresponded to an estimated 0.0254 increase in dry-condition FS.

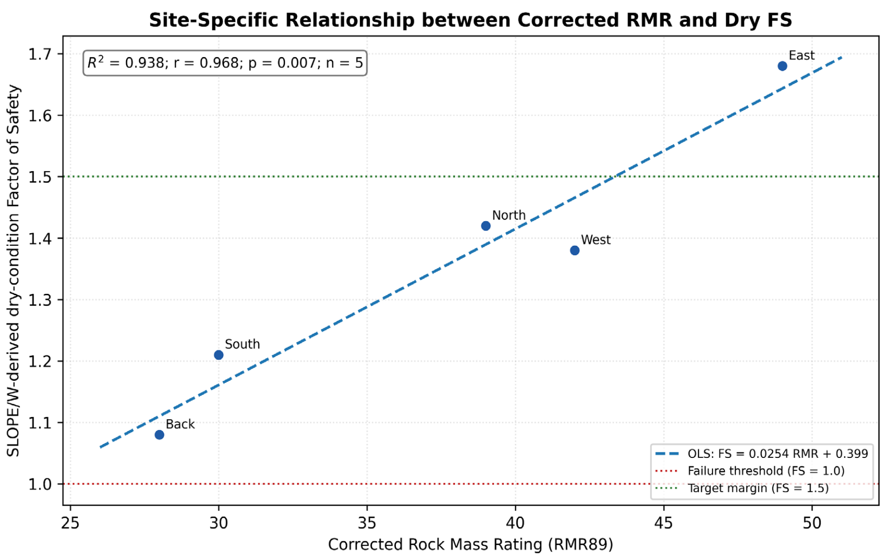

Figure 7. Exploratory relationship between corrected RMR89 and SLOPE/W-derived dry-condition Factor of Safety for five quarry walls. The fitted line summarizes the site dataset and is not an independent predictive validation.

4.6.2. Pearson Correlation Results

Pearson's correlation was strongly positive (r = 0.9683; t(3) = 6.714; two-sided p = 0.0067; n = 5). The Fisher-transformed approximate 95% confidence interval was 0.590 - 0.998; its breadth reflects the very small sample. In simple one-predictor OLS, the test of zero slope and the Pearson test of zero correlation are mathematically equivalent, so they are two descriptions of the same association rather than independent confirmatory tests.

The relationship is therefore interpreted only as a site-specific summary. RMR-related properties partly inform the SLOPE/W inputs, the five walls do not provide an external validation set, and the North and West walls cannot be treated as independent validation cases after contributing to model fitting. The equation should not be transferred to design at other quarries without independent observations and calibration.

4.7. Descriptive Stability-Group Comparison

The failure-prone subgroup as shown in Figure 8 comprises the South and Back walls because saturated FS is below 1.0 and both show pronounced cracking or recurrent instability. Their corrected RMR values are 30 and 28, giving a mean of 29.0 (n = 2). The comparatively stable/marginal subgroup comprises North, East and West, with RMR values of 39, 49, and 42 and a mean of 43.3 (n = 3). The 14.3-point difference is consistent with poorer rock mass at the failure-prone walls. No inferential group-comparison test is reported because the groups contain only two and three independent wall-scale observations; group differences are therefore interpreted descriptively.

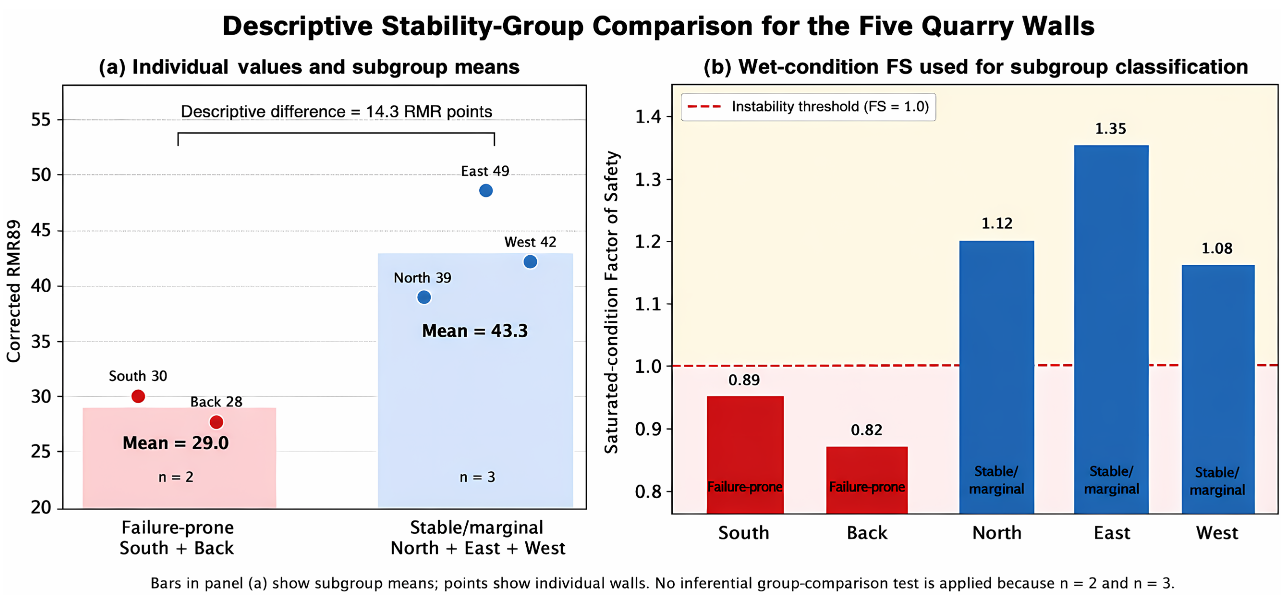

Figure 8. Descriptive comparison of the failure-prone subgroup (South and Back) and the stable/marginal subgroup (North, East and West). Panel (a) shows corrected RMR89 values, individual walls and subgroup means (29.0, n = 2; 43.3, n = 3; difference = 14.3 points). Panel (b) shows wet-condition FS values and the FS = 1.0 instability threshold used for subgroup classification. No inferential group-comparison test was applied because of the small subgroup sizes.

4.8. Geological Hazard Prioritization Matrix

The integrated assessment identified the Back and South walls as the highest-priority intervention zones. The Back Wall combines Poor rock (RMR = 28), the lowest wet-condition FS (0.82), a 28 m height and a 75˚ face. The South Wall also has Poor rock (RMR = 30) and a wet-condition FS below unity (0.89). The North Wall remains Poor rock (RMR = 39) and marginal under the wet scenario (FS = 1.12). The West and East walls are Fair rock (RMR = 42 and 49) with wet-condition FS values of 1.08 and 1.35, respectively. These categories are screening priorities derived from the combined RMR, SLOPE/W, groundwater, deformation and rockfall evidence; they are not failure probabilities.

These findings indicate that geological hazard increases progressively with declining rock mass quality, steeper slope angles, greater excavation heights, and groundwater-induced reductions in stability. The integrated hazard prioritization matrix (Figure 9) synthesizes these geotechnical and geological parameters into a practical engineering tool for ranking slope instability risk and guiding stabilization, monitoring, and maintenance priorities at Kaseve Quarry. The matrix is intended as a site-specific decision-support framework rather than a probabilistic prediction model.

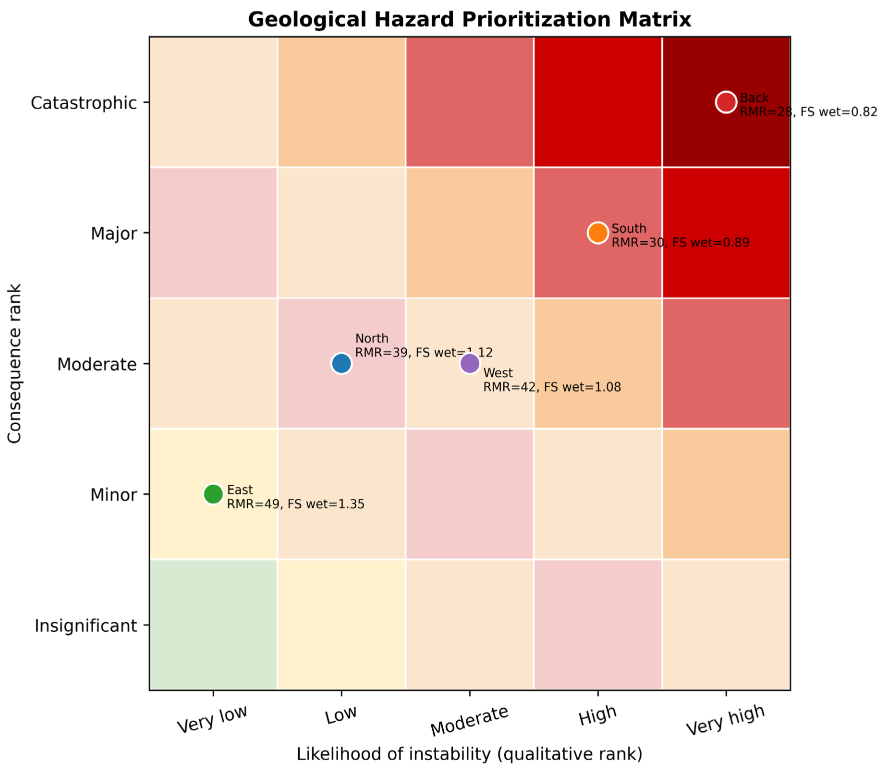

Figure 9. Qualitative geological-hazard prioritization matrix integrating corrected RMR89, wet-condition FS, mapped deformation, groundwater evidence and recorded rockfalls. Likelihood and consequence ranks are ordinal site-screening scores, not failure probabilities.

5. Discussion

5.1. Rock-Mass Quality and Wall Geometry

Corrected RMR89 values at Kaseve Quarry range from 28 to 49, placing the Back, South and North walls in Class IV (Poor rock) and the West and East walls in

Class III (Fair rock). The range is consistent with the mapped variability in weathering, discontinuity spacing and discontinuity condition. The Back Wall is of particular concern because its Poor-rock classification coincides with the greatest wall height, steepest face, highest adopted wet-season pore pressure and lowest SLOPE/W-derived wet-condition FS.

RMR classification alone does not prescribe a universal safe face angle. The present wall geometries should instead be evaluated using wall-specific kinematic analysis, Slope Mass Rating where applicable, and the limit-equilibrium models described in Section 3.4. The 75˚ Back Wall and 72˚ South Wall merit priority review because their steep geometry occurs together with Poor rock, wet-condition FS below 1.0 and field evidence of instability.

5.2. Factor of Safety and Seasonal Failure Risk

The SLOPE/W results show reductions of 0.26 - 0.33 between the dry and adopted wet scenarios, demonstrating the sensitivity of the modelled walls to seasonal pore pressure. The Back-Wall FS decreases from 1.08 to 0.82 and the South-Wall FS from 1.21 to 0.89. Historical records identify 17 wall-specific rockfall entries during 2015-2021, including seven at the Back Wall.

The South Wall wet-condition FS of 0.89 is operationally important because this wall is an active extraction face. Its 72˚ face, 20 m height, low effective cohesion (22 kPa), mapped daylighting structure and elevated wet-season pore pressure warrant access controls, drainage and displacement monitoring. Rainfall-triggered restrictions should be tied to observable thresholds such as accelerating crack movement, fresh rockfall or abrupt pore-pressure rise, rather than to an uncalibrated standalone FS trigger.

5.3. Regression Model and Predictive Value

For the corrected dataset, FS = 0.0254 × RMR + 0.399 ($R^2 = 0.938$; $r = 0.968$; $p = 0.007$; $n = 5$). The fit is strong within the five analysed walls, but the result is exploratory and site-specific. Because RMR-related material properties contribute to the SLOPE/W calculations, the association is partly model-structured and must not be interpreted as independent proof that RMR alone predicts stability. External validation using more walls and independent sites is required before predictive use.

5.4. Blasting Damage and Cumulative Hazard

Repeated blasting may progressively damage exposed rock by opening pre-existing discontinuities and reducing block interlock; however, the present dataset does not quantify a time-dependent reduction in RMR. Blasting is therefore considered a plausible cumulative stressor rather than a quantitatively isolated driver of rock-mass deterioration. The corrected Back and South ratings are 28 and 30, both within Class IV (Poor rock). Their intervention priority follows from the combined rock-mass, SLOPE/W, groundwater, deformation and rockfall evidence, not from a purported critical RMR threshold of 28.

5.5. Engineering and Regulatory Implications

Immediate measures should include access exclusion below the Back and South walls, removal of loose blocks, crest-water diversion, drainage, re-benching, and reduction of unsupported face angles. Medium-term measures should include additional piezometers, crack gauges, periodic drone surveys and annual repeat RMR mapping. Quarry production should be suspended at critical walls during intense rainfall or where rapid crack movement, fresh rockfall, or abrupt pore-pressure rise is observed.

5.6. Contextual Comparison with East African Quarrying Studies

The findings add a quantitative site-scale example to the limited published discussion of quarry geohazards in Machakos County. Comparisons with other East African quarry studies should remain qualitative unless those studies report directly comparable RMR89 components, wall geometries, hydraulic assumptions and limit-equilibrium methods.

6. Conclusions and Recommendations

This study presents an integrated quantitative geotechnical assessment of slope stability at Kaseve Quarry, Machakos County, Kenya, combining corrected Rock Mass Rating (RMR89), SLOPE/W-derived Factor of Safety, historical quarry-management records and field-based geological-hazard observations. The findings provide an engineering evidence base for evaluating slope stability, identifying higher-priority wall sections and targeting risk-reduction measures.

6.1. Key Findings

1) Rock mass quality varied considerably across the quarry, with RMR values ranging from 28 to 49, classifying the investigated quarry wall sections as either Poor (Class IV) or Fair (Class III) according to the Bieniawski classification system. The Back Wall (RMR = 28) and South Wall (RMR = 30) exhibited the poorest rock mass quality, whereas the East Wall (RMR = 49) demonstrated the most competent rock mass conditions.

2) Groundwater conditions strongly influenced slope stability. Dry-condition Factor of Safety (FS) values ranged from 1.08 to 1.68, while saturated-condition FS values declined to 0.82 - 1.35, with the Back Wall (FS = 0.82) and South Wall (FS = 0.89) falling below the critical stability threshold (FS < 1.0). These results demonstrate the significant influence of seasonal pore-water pressure on quarry slope stability.

3) Corrected rock-mass quality showed a strong site-specific association with dry-condition stability. The fitted model (FS = 0.0254RMR + 0.399; $R^2 = 0.938$; r = 0.968; p = 0.007; n = 5) summarizes the five analysed walls. Because RMR-related properties contribute to the SLOPE/W inputs and the sample is small, the

relationship is exploratory and should not be transferred to predictive design without independent validation.

4) Field observations corroborated the analytical results. Tension cracks, progressive crack widening, groundwater seepage, blast-induced fracturing, and documented rockfall occurrences were concentrated at the Back and South Walls, confirming these sections as the highest-priority intervention zones for slope stabilization.

5) The integration of historical records (2015-2021) with detailed geotechnical investigations (2022-2024) provided a comprehensive understanding of long-term slope behavior and demonstrated the value of combining operational records with quantitative engineering analyses for quarry hazard assessment.

6.2. Engineering Recommendations

Based on the findings of this study, the following measures are recommended to improve quarry safety and long-term slope stability:

1) Re-bench and flatten the Back and South quarry walls to achieve geometries compatible with their rock mass quality and stability characteristics.

2) Install surface and subsurface drainage systems to reduce seasonal pore-water pressures and minimize rainfall-induced instability.

3) Implement controlled blasting techniques to limit blast-induced fracturing and progressive deterioration of rock mass quality.

4) Establish a continuous geotechnical monitoring programme incorporating crack gauges, standpipe piezometers, drone-based photogrammetry, and periodic Rock Mass Rating reassessments.

5) Restrict personnel access and suspend quarry operations beneath critical slopes during periods of intense rainfall or where monitoring indicates rapid crack propagation, elevated groundwater levels, or increased rockfall activity.

6) Extend similar integrated RMR-factor of safety investigations to other hard-rock quarries within the Mozambique Belt and comparable crystalline basement terrains to support regional quarry safety guidelines and regulatory decision-making.

Acknowledgements

The authors thank the Almighty God for guidance and wisdom. Appreciation is extended to Dr. Mary Mwangi and Dr. Julian Awuor Ogondo for academic guidance, Kaseve Quarry management and workers for site access and cooperation, and Grad. Geol. Ahsanat Ndunge for GIS support. Field investigations were supported through the South Eastern Kenya University postgraduate research program.

Author Contributions

Charles Ngala Kithome: Conceptualization, methodology, investigation, field data collection, formal analysis, visualization, and writing-original draft. Julian A.

Ogondo: Supervision, methodology review, validation, and writing-review and editing. Mary Mwangi: Supervision, methodology review, validation, and writing-review and editing. All authors reviewed and approved the final manuscript.

Conflicts of Interest

The authors declare no conflicts of interest regarding the publication of this paper.

References

Bieniawski, Z. T. (1989). *Engineering Rock Mass Classifications: A Complete Manual for Engineers and Geologists in Mining, Civil, and Petroleum Engineering.* Wiley.

Christopher M. Indiatsy, (2018). Analysis of Historical Monthly, Seasonal and Annual Rainfall Variability (1990-2014) in Machakos Sub County, Kenya. *International Journal of Multidisciplinary and Current Research, 6,* 24-41. https://doi.org/10.14741/ijmcr.v6i01.10904

Deere, D. U., & Miller, R. P. (1966). *Engineering Classification and Index Properties of Intact Rock (Technical Report AFWL-TR-65-116).* Air Force Weapons Laboratory.

Fredrick, K. O., Mwakumanya, M. A., & Tole, M. P. (2023). Slope Stability Analysis at Soapstone Mining Sites in Nyamarambe, Kisii County, Kenya. *International Journal of Geography, Geology and Environment, 5,* 95-110. https://doi.org/10.22271/27067483.2023.v5.i2b.177

Fritz, H., Abdelsalam, M., Ali, K. A., Bingen, B., Collins, A. S., Fowler, A. R. et al. (2013). Orogen Styles in the East African Orogen: A Review of the Neoproterozoic to Cambrian Tectonic Evolution. *Journal of African Earth Sciences, 86,* 65-106. https://doi.org/10.1016/j.jafrearsci.2013.06.004

Mathu, E. M. (1992). The Mutito and Ikoo Faults in the Pan-African Mozambique Belt, Eastern Kenya. In R. Mason (Ed.), *Basement Tectonics 7* (pp. 61-69). Springer. https://doi.org/10.1007/978-94-017-0833-3_5

Nyamai, C., Mathu, E., Opiyo-Akech, N., & Wallbrecher, E. (2004). A Reappraaisal of the Geology, Geochemistry, Structures and Tectonics of the Mozambique Belt in Kenya, East of the Rift System. *African Journal of Science and Technology, 4,* 51-71. https://doi.org/10.4314/ajst.v4i2.15306

Palmström, A. (1982). The Volumetric Joint Count: A Useful and Simple Measure of the Degree of Rock Mass Jointing. In *Proceedings of the 4th International Congress of the International Association of Engineering Geology* (pp. 221-228). A. A. Balkema.

Ulusay, R., & Hudson, J. A. (Eds.). (2007). *The Complete ISRM Suggested Methods for Rock Characterization, Testing and Monitoring: 1974-2006*. ISRM Turkish National Group.